A Letters Journal Exploring the Frontiers of Physics

January 2020

EPL, **129** (2020) 17001
doi: 10.1209/0295-5075/129/17001

www.epljournal.org

Dynamic response of partially spin- and valley-polarised two-dimensional electron liquids

Maximilian Schober, Dominik Kreil and Helga M. Böhm

Institute for Theoretical Physics, Johannes Kepler University - Linz, Austria

received 10 September 2019; accepted in final form 4 January 2020
published online 12 February 2020

PACS 73.20.Mf – Collective excitations (including excitons, polarons, plasmons and other charge-density excitations)
PACS 73.21.Fg – Quantum wells
PACS 73.21.-b – Electron states and collective excitations in multilayers, quantum wells, mesoscopic, and nanoscale systems

Abstract – The growing field of valleytronics provides new promising physics. Here, we focus on the collective modes of an infinitely thin electron layer with a binary valley degree of freedom that is unequally occupied. The spin populations are allowed to be imbalanced, too. This system can support four collective modes and two anti-resonances emerge. We study this copious dynamics in the spin- and valley-sensitive random phase approximation (RPA) and explain the uncommon behaviour by building a bridge from the many-fermion system to its bosonic counterpart. For completeness, we also report the RPA exchange and correlation energies for arbitrary spin and valley polarisation. A phase transition occurs at $r_S \approx 6$ from the four-component to the ferromagnetic, single-valley-occupation state.

Introduction. – For decades, two-dimensional (2D) electron liquids in semiconductor heterostructures and inversion layers [1] have opened the doors to numerous new devices. The recent successful preparation of new classes of 2D materials (such as graphene, silicene, and transition metal dichalcogenide (TMD) layers) [2–5], has triggered a revival of the field, offering even more application prospects [6–10]. This implies the necessity to better understand the physics of unprecedented *collective modes* occurring in these systems.

In addition to charge $\pm e$ and spin σ, the electrons or holes are further characterised by their "valley" index τ, referring to degenerate but inequivalent band structure extrema, well separated in momentum ($\mathbf{q}$) space. Robust against low-energy perturbations, τ forms an independent degree of freedom (DoF) or "pseudospin".

In monolayer TMDs, strong spin-orbit coupling (SOC) and time reversal symmetry connect spin and valley [5], allowing to individually address τ statically (by Zeemann splitting) and dynamically (via the helicity of photons). Such manipulations aim at employing σ and τ as information carriers ("solid state qubits"). This usage is known as spintronics and valleytronics, respectively.

In conventional Si [100] 2D electron liquids (2DELs), the six bulk conduction band valleys are split [11,12] due to the different effective mass perpendicular to the interface into 4 plus 2; similar splittings affect the valence band maxima of most semiconductors. All these valleys can be further raised or lowered by (usually uni- or biaxial) stress, which is thus well suited to control their occupancy [12,13]. Recently, Renard *et al.* [14] achieved to valley-polarise a Si 2DEL, which in contrast to strained AlAs [15] has an isotropic in-plane effective mass.

In such electron layers, studies on the valley DoF dating back to the 1970s [16,17] have established the importance of many-body (MB) correlations. Prominent examples, among others, are the influence of τ on the spin susceptibility [15,18,19] and vice versa [20], on the effective mass [21], and a possible phase transition to full valley polarisation [17,22,23]. Here, we point out another remarkable MB effect, relevant for the *dynamical* response of the system, namely the occurrence of new as well as the suppression of familiar excitation modes.

Based on the random phase approximation (RPA) for the partially spin-polarised single-valley 2DEL, Agarwal *et al.* [24] predicted a long-lived spin-plasmon. In a more advanced approach [25,26] it is substantially lowered in energy $\hbar\omega$; further, a significant gap emerged in the particle-hole excitations of the majority spins, where magnetic perturbations cannot influence their behaviour.

A 2DEL with partial polarisation in both spin *and* valley allows an even richer excitation structure governed by the components' relative weight. Our purpose here is to elucidate the features in the (q,ω) plane. Of course, the location of peaks and gaps depends on the single-particle energy dispersion (linear as in graphene[1] and monolayer TMDs or quadratic as in semiconductor quantum wells) and is expected to be considerably influenced by SOC. To cover the essence of the remarkable dynamical attributes, however, we prefer to refrain from all specific material aspects and study the simplest prototype, a homogeneous 2DEL with valleys $\tau = \pm$ and spins $\sigma = \uparrow, \downarrow$ at zero temperature and zero width, where excitations to higher subbands [28,29] can be ignored. In the same spirit we neglect disorder and use the RPA, providing a qualitatively correct excitation spectrum over a wide (q,ω) region. Our aim is to explain the various unfamiliar, pronounced collective modes. The inclusion of SOC [30] and extension to Dirac materials would be the next logical steps.

Partial response functions. – The key properties of the theory are the various linear response functions. They can be decomposed into their partial components $\chi_{\lambda\lambda'}(q,\omega)$, where we combine the quantum numbers $(\sigma,\tau) \equiv \lambda$ to guarantee better readable equations. Linear combinations then give the experimentally relevant response functions $\chi_{[ab]}(q,\omega)$, with a, b denoting observables coupled to the applied external perturbations; specifically, here particle density n, spin density s, valley density v, and helical density h couple to voltage, magnetic field, stress, and circular light polarisation, respectively.

In table 1 all involved densities are listed. Partially polarised systems have cross-correlations implying $\chi_{[ab]} \neq 0$ for $a \neq b$ (*e.g.*, pure stress or an electrostatic potential can induce a spin density change δs). The same four distinct peaks show up in all the corresponding response functions, but with different strengths. If in $\chi_{[aa]}$ such a collective mode is dominant for small and perceptible for all polarisations, we refer to it as the "a-plasmon" (see table 1 and the discussion below).

The imbalances of the partial densities determine the polarisations. These read (with $\mathrm{sgn}(\lambda) \equiv \mathrm{sgn}(\sigma\tau)$)

$$\begin{aligned} n &= \sum_\lambda n_\lambda, \\ s &= \sum_\lambda \mathrm{sgn}(\sigma) n_\lambda \equiv n\zeta_\sigma, \\ v &= \sum_\lambda \mathrm{sgn}(\tau) n_\lambda \equiv n\zeta_\tau, \\ h &= \sum_\lambda \mathrm{sgn}(\lambda) n_\lambda \equiv n\zeta_\gamma. \end{aligned} \tag{1}$$

The particle density n is conventionally expressed via the Wigner-Seitz radius $r_\mathrm{S} a_\mathrm{B}^* \equiv (\pi n)^{-1/2}$, where a_B^* is the effective Bohr radius of a material with effective mass m^*.

Table 1: Partial density (n_λ) combinations "a" coupling to external perturbations. Each $\mathrm{Im}\chi_{[aa]}$ is dominated by one specific mode (right column). We expect the last one to be strong in SOC materials.

$n = n_{+\uparrow} + n_{+\downarrow} + n_{-\uparrow} + n_{-\downarrow}$	$\chi_{[nn]}$	charge-plasmon
$s = n_{+\uparrow} - n_{+\downarrow} + n_{-\uparrow} - n_{-\downarrow}$	$\chi_{[ss]}$	spin-plasmon
$v = n_{+\uparrow} + n_{+\downarrow} - n_{-\uparrow} - n_{-\downarrow}$	$\chi_{[vv]}$	valley-plasmon
$h = n_{+\uparrow} - n_{+\downarrow} - n_{-\uparrow} + n_{-\downarrow}$	$\chi_{[hh]}$	helicity-plasmon

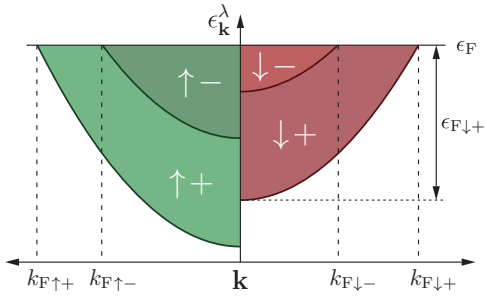

Fig. 1: Single-particle energies. The distance of the respective band minimum to ϵ_F is $\epsilon_{\mathrm{F}\lambda} \equiv \hbar^2 k_{\mathrm{F}\lambda}^2/(2m^*)$.

At zero temperature, all states $|\mathbf{k}\lambda\rangle$ of the non-interacting ground state are filled to the Fermi energy $\epsilon_\mathrm{F} \equiv \hbar^2 k_\mathrm{F}^2/(2m^*)$, defining a "mean" Fermi momentum. The actual Fermi circles of the partial densities are $k_{\mathrm{F}\lambda}^2 = 4\pi n_\lambda$, or equivalently, $k_{\mathrm{F}\lambda} = k_\mathrm{F}\sqrt{1 \overset{+}{(-)} \zeta_\sigma}\sqrt{1 \overset{+}{(-)} \zeta_\tau}$. The sign $\overset{+}{(-)}$ reflects the choice of majority particles as having spin $\uparrow$ and valley index $+$, respectively (see fig. 1).

Without partial polarisation, the total degeneracy factor $g_\mathrm{f} \equiv g_\mathrm{s} g_\mathrm{v} \equiv 4\pi n/k_\mathrm{F}^2$ can take the values 4 (para-spin and para-valley state $g_\mathrm{s} = 2 = g_\mathrm{v}$), 2 (ferro-spin and para-valley or vice versa), and 1 (if both, $\zeta_\sigma = \zeta_\tau = 1$).

We only allow for spin- and valley-conserving excitations[2] (longitudinal and transverse responses can be separated via the scattered photon properties in Rahman spectroscopy, where the response functions of table 1 are combined with different ζ_λ^n prefactors [32]).

A homogeneous 2DEL consists of N_λ charge carriers with a single-particle basis $|\mathbf{k}\lambda\rangle$ and energies $\epsilon_\mathbf{k}^\lambda$, where λ encompasses all discrete quantum numbers. Examples are $(\sigma\tau)$ as above, (σs) with s denoting valence and conduction band, or $(\gamma\tau s)$ in valley-polarised graphene with SOC[3] and helicity DoF γ. The generic expression for the non-interacting partial response functions (Lindhard functions) of these multi-component fermion systems reads

[1] The dynamics with a tight-binding dispersion for unpolarised graphene was studied in [27].

[2] For intervalley plasmons, see ref. [31].

[3] σ is no longer a good quantum number.

($n(\epsilon)$ is the Fermi distribution and $\Delta\epsilon^{\lambda\lambda'}_{\mathbf{k},\mathbf{k}+\mathbf{q}} \equiv \epsilon^{\lambda'}_{\mathbf{k}+\mathbf{q}} - \epsilon^{\lambda}_{\mathbf{k}}$)

$$\chi^0_{\lambda\lambda'}(q,\omega) \equiv \frac{n_\lambda}{N_\lambda}\sum_{\mathbf{k}} f^{\lambda\lambda'}_{\mathbf{k},\mathbf{k}+\mathbf{q}} \frac{n(\epsilon^{\lambda}_{\mathbf{k}}) - n(\epsilon^{\lambda'}_{\mathbf{k}+\mathbf{q}})}{\hbar\omega + \mathrm{i}0^+ - \Delta\epsilon^{\lambda\lambda'}_{\mathbf{k},\mathbf{k}+\mathbf{q}}} \quad (2)$$

(the small imaginary contribution ensuring causality). The factor $f^{\lambda\lambda'}_{\mathbf{k},\mathbf{k}+\mathbf{q}}$ is the squared overlap between initial and final single-particle states.

It is convenient to extend $\omega \to z$ in the complex plane and define characteristic (q,z) lines; we express these in reduced units, measuring wave vectors $\bar{q}_\lambda$ in $k_{\mathrm{F}\lambda}$ and energies $\hbar\bar{\omega}_\lambda$ in $\epsilon_{\mathrm{F}\lambda}$; the response functions $\bar{\chi}_{\lambda\lambda'}$ are scaled with $\epsilon_{\mathrm{F}\lambda}/n_\lambda$, equal to the inverse of the density of states D_0 at the Fermi surface (constant in 2D, $D_0 \equiv m^*/(2\pi\hbar^2)$).

For the partial Lindhard functions of an isotropic 2DEL with parabolic energy dispersion, the overlap is simply $\delta_{\lambda\lambda'}$, and the evaluation results in [1]

$$\bar{\nu}^{\pm}(\bar{q},\bar{z}) \equiv \bar{q}/2 \pm \bar{z}/(2\bar{q}), \quad \bar{\nu}^{\pm}_\lambda \equiv \bar{\nu}^{\pm}(\bar{q}_\lambda,\bar{z}_\lambda), \quad (3a)$$

$$\Psi^{\pm}(z) \equiv \pm\mathrm{sgn}(\mathrm{Re}z)\sqrt{z^2-1} \mp z, \quad (3b)$$

$$\bar{\chi}^0_{\lambda\lambda'}(q,\omega) = \delta_{\lambda\lambda'}\frac{1}{\bar{q}_\lambda}[\Psi^+(\nu^+_\lambda) + \Psi^-(\nu^-_\lambda)]. \quad (3c)$$

We will further abbreviate $\chi^0_\lambda \equiv \chi^0_{\lambda\lambda}$. The full free response functions all coincide, $\chi^0_{[nn]} = \chi^0_{[ss]} = \chi^0_{[vv]} = \chi^0_{[hh]} \equiv \chi^0$.

In graphene, $\chi^0_{\lambda\lambda'}$ is diagonal, too. Neglecting SOC, the main qualitative difference to quantum wells are the additional, gapless interband particle-hole excitations. They cause strong Landau-damping of collective modes, especially for partial spin or valley polarisation.

Random phase approximation. – The valley separation in momentum space is typically much larger than k_{F} so that inter-valley scattering can be ignored. Combining the partial response functions $\chi_{\lambda\lambda'}$ into the matrix $\underline{\underline{\chi}}$, the RPA takes the form

$$\underline{\underline{\chi}} = \left[\underline{\underline{1}} - \underline{\underline{\chi^0}} \cdot \underline{\underline{V}}\right]^{-1} \cdot \underline{\underline{\chi^0}}. \quad (4)$$

Here, all entries in $\underline{\underline{V}}$ are the bare Coulomb interaction in momentum space, $v(q) = 2\pi e^2/(q\varepsilon_{\mathrm{b}})$; with ε_{b} the background dielectric constant. For the areal densities realised in most 2DELs [33,34], the RPA is a decent choice and arguably gets better with increasing degeneracy g_{f} [1]. For our aim, the "landscape" of small q collective modes, the RPA is certainly the prime starting point.

Since all $V_{\lambda\lambda'}$ are identical, the determinant in the matrix equation (4) simplifies to $\Delta(q,\omega) \equiv 1 - v(q)\chi^0(q,\omega)$, resulting in the partial RPA response functions

$$\chi^{\mathrm{RPA}}_{\lambda\lambda'} = \chi^0_\lambda\,\delta_{\lambda\lambda'} + v\chi^0_\lambda\chi^0_{\lambda'}/\Delta. \quad (5a)$$

The free response of the λ-constituents is augmented by a $v(q)$-proportional term, coupling the fluctuations $\chi^0_\lambda\,\chi^0_{\lambda'}$. All partial responses share the denominator $\Delta(q,\omega)$. Suitable scaling factors[4] are now the mean k_{F} and ϵ_{F},

$$\overline{\chi}^{\mathrm{RPA}}_{\lambda\lambda'} = \frac{\bar{\chi}^0_\lambda}{g_{\mathrm{f}}\,\Delta}\Big(\delta_{\lambda\lambda'} + \frac{r_{\mathrm{S}}\sqrt{g_{\mathrm{f}}}}{2\overline{q}}\left(\bar{\chi}^0_{\lambda'} - \bar{\chi}^0\delta_{\lambda\lambda'}\right)\Big). \quad (5b)$$

The full response functions $\chi_{[ab]}$ of experimental interest are all combinations of $a,b \in \{n,s,v,h\}$. We define coefficients $\alpha^{ab}_{\lambda\lambda'} = \pm 1$ with the help of eq. (1) and obtain

$$\left.\begin{aligned} a &= \sum_\lambda \alpha^a_\lambda\, n_\lambda \\ b &= \sum_{\lambda'} \alpha^b_{\lambda'}\, n_{\lambda'} \end{aligned}\right\} \quad \chi^{\mathrm{RPA}}_{[ab]} = \sum_{\lambda\lambda'} \alpha^{ab}_{\lambda\lambda'}\chi^{\mathrm{RPA}}_{\lambda\lambda'}. \quad (6)$$

In $\chi_{[nn]}$ all $\alpha^{nn}_{\lambda\lambda'} = 1$, yielding the density induced by an external voltage; the longitudinal spin-density fluctuations due to an external magnetic field are obtained with $\alpha^{ss}_{\lambda\lambda'} = \mathrm{sgn}(\sigma\sigma')$; analogoulsy, $\alpha^{vv}_{\lambda\lambda'} = \mathrm{sgn}(\tau\tau')$ yields the valley-valley response. From eq. (5b) it is clear that either combination $\chi_{[ab]}$ has the same poles, given by the zeroes of the RPA dielectric function.

In the fully unpolarised (para-magnetic and para-valley) case, all $k_{\mathrm{F}\lambda}$ coincide, thus $\chi^0_\lambda = \chi^0/g_{\mathrm{f}}$ and only $\chi_{nn} = \chi^0/\Delta$ differs from the non-interacting result. For partially polarised 2DELs the RPA cross-response functions with $a \neq b$ become relevant, in contrast to their vanishing counterparts $\chi^0_{[ab]}$. For example,

$$\begin{aligned}\chi^{\mathrm{RPA}}_{[sv]} = \frac{1}{\Delta}\{&\chi^0_{\uparrow+} + \chi^0_{\downarrow-} - \chi^0_{\downarrow+} - \chi^0_{\uparrow-} \\ &-4v(q)\left(\chi^0_{\uparrow+}\,\chi^0_{\downarrow-} - \chi^0_{\downarrow+}\,\chi^0_{\uparrow-}\right)\}\end{aligned} \quad (7)$$

causes a modulation of the spin-density $s(\mathbf{r})$ in real space solely by applying stress; vice versa, the valley occupancy density $v(\mathbf{r})$ can be changed by a magnetic field (recall that this happens without SOC).

Before discussing the resulting rich excitation spectrum, we briefly comment on the RPA energy.

RPA ground-state energy. – The phase diagram of the 2DEL has proved tricky for decades. Certainly, there exist much better studies [35,36] on the ground-state energy ε_g per particle than the RPA. But we consider it adequate to report ε_g for completeness and comparison.

The presence of an additional DoF, equivalent to spin, weakens the impact of the Pauli principle, changing ε_g significantly, as the number of possible exchange partners gets lowered. In the bare RPA (in contrast to approaches with effective interactions $V_{\lambda\lambda'}(q)$), valley and spin are equivalent. The free kinetic and exchange contributions, $\varepsilon^0_{\mathrm{kin}}$ and $\varepsilon_{\mathrm{exc}}$, are readily computed and read (in Rydberg):

$$\varepsilon^0_{\mathrm{kin}} = \frac{1}{2r_{\mathrm{S}}^2}(1+\zeta_\sigma^2)(1+\zeta_\tau^2), \quad (8)$$

$$\varepsilon_{\mathrm{exc}} = \frac{-2}{3\pi r_{\mathrm{S}}}\sum_{\sigma\tau}((1+\mathrm{sgn}(\sigma)\zeta_\sigma)(1+\mathrm{sgn}(\tau)\zeta_\tau))^{3/2}. \quad (9)$$

[4] We denote this with a long overline. In 2D, $n_\lambda/\epsilon_{\mathrm{F}\lambda} = D_0 = g_{\mathrm{f}}n/\epsilon_{\mathrm{F}}$, so that all $\overline{\chi} = \bar{\chi}/g_{\mathrm{f}}$.

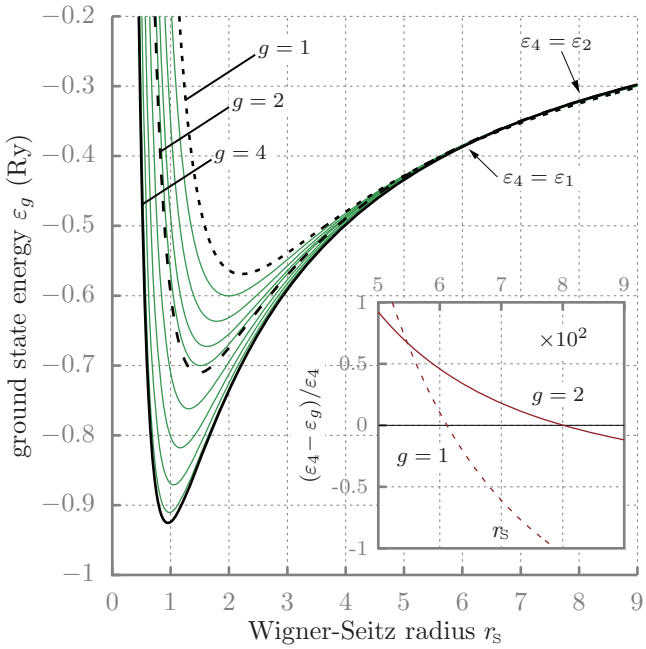

Fig. 2: RPA energy per particle for partial polarisations in steps of 0.2 (green lines from bottom to top) with ζ_σ: $0 \to 1$ and then ζ_τ: $0 \to 1$. Black full, dashed and dotted line: $(\zeta_\sigma, \zeta_\tau) = (0,0)$, $(0,1)$ and $(1,1)$, respectively.

For the correlation part $\varepsilon_{\rm cor}$ we utilise the Hellman-Feynman theorem (or scaled potential approach); abbreviating $Q^0(q,\omega) \equiv -v(q)\chi^0(q,\omega)$, this results in a two-dimensional integral, to be evaluated numerically,

$$\varepsilon_{\rm cor} = \frac{\hbar}{4\pi^2 n} \int_0^\infty q{\rm d}q \int_0^\infty {\rm d}\omega \, (\ln[1 + Q^0(q,\omega)] - Q^0(q,\omega)). \tag{10}$$

The ground-state energy, $\varepsilon_g = \varepsilon^0_{\rm kin} + \varepsilon_{\rm exc} + \varepsilon_{\rm cor}$, depends on $r_{\rm S}$ and symmetrically[5] on the partial polarisations $(\zeta_\sigma, \zeta_\tau)$. The cases $\zeta = 0$ and 1 have been frequently investigated with regard to a possible phase transition (PT) from $g_{\rm f} = 2 \equiv g_2$ (spins $\uparrow, \downarrow$ in a single-valley or a ferromagnetic 2-valley 2DEL) to $g_{\rm f} = 1 \equiv g_1$ (ferromagnetic 1-valley case [36,38]), or, similarly, a PT from $g_{\rm f} = 4 \equiv g_4$ (fully unpolarised spins $\uparrow, \downarrow$ in 2 valleys) to g_2 [22,35,36,39]. The latter comparison is of particular importance, because such a "valley PT" could explain conductance measurements in Si [23,40].

We display ε_g in fig. 2 for increasing ζ, changing the 2DEL from $g_4 \to g_1$. As is well known, for high $r_{\rm S}$ the energies get extremely close, yielding PTs due to the screened Coulomb interaction, depending on the local exchange hole. The fully valley-polarised, paramagnetic g_2 system is energetically preferred to g_4 for $r_{\rm S} \geq 8$ (see inset of fig. 2). Such a $r_{\rm S} \approx 8$ valley occupancy PT was suggested in the 90s, based on both experiments [41] and calculations [39]. Note, however, that the RPA g_1 phase is even lower in energy for densities below $r_{\rm S} = 6.1$ ($n \approx 1.9 \times 10^{11}\,{\rm cm}^{-2}$, $k_{\rm F} \approx 3.9 \times 10^5\,{\rm cm}^{-1}$ for a typical Si sample).

[5] Experiments on m^* contradict this feature of the bare RPA [37].

Table 2: Negative ε_{xc} at densities clearly distinct from the PT values: numerical RPA result, error of the RPA fit (eq. (11) with $a_0 = -2.05429$, $b_0 = 0.582439$); MC fits (as cited in the column header), and error of $\varepsilon_{xc}^{\rm RPA}$ compared to MC. Note that the latter is hardly influenced by the degeneracy.

$r_{\rm S}$	$g_{\rm f}$	RPA	% fit	MC [36]	MC [44]	% err.
2	4	0.8608	−0.51	0.7116	–	−21.6
	2	0.9244	0.29	0.7662	0.7669	−20.2
	1	1.0638	0.33	–	0.8806	−20.4
7	4	0.3606	−0.59	0.2438	–	−48.8
	2	0.3702	−0.58	0.2501	0.2501	−48.9
	1	0.3933	0.07	–	0.2634	−49.2
10	4	0.2829	−0.54	0.1773	–	−60.4
	2	0.2885	−0.63	0.1806	0.1806	−60.7
	1	0.3020	−0.24	–	0.1873	−61.7

Based on the RPA property $\varepsilon_{xc}(r_{\rm S}, g_{\rm f}) = g_{\rm f}\, \varepsilon_g(g_{\rm f}^{3/2} r_{\rm S}, 1)$ we fit the energies with $x \equiv 1/(2r_{\rm S})^{2/3}$ to the simple form

$$\varepsilon_{\rm xc}(r_{\rm S}, \zeta) = \frac{a_0 x}{1 - \frac{b_0}{\gamma(\zeta_\sigma)\gamma(\zeta_\tau)} x}, \tag{11}$$
$$\gamma(\zeta) \equiv 2/\big(1 + (2^{3/4} - 1)\zeta^2\big)^{4/3},$$

valid for $r_{\rm S} \geq 2$. The error is reported in table 2, where we also compare with Monte Carlo (MC) energies[6] [36,44].

Resonances and anti-resonances. – The common denominator of the RPA response functions, $\Delta = 1 - v\chi^0$, equals the determinant of the 4×4 matrix $\underline{\underline{1}} - \underline{\underline{\chi^0}} \cdot \underline{\underline{V}}$. This defines 4 collective modes, noticeable in all $\chi_{[ab]}$, including the cross-response functions $[a \neq b]$. These "plasmons", listed in table 1, are often sloppily defined by $\Delta(q,\omega) = 0$. This, however, requires more care.

As seen in the left panel of fig. 3, ${\rm Re}\Delta(q,\omega)$ crosses zero 8 times (a colour change red $\leftrightarrow$ blue at steep or a white region at low variations); two adjacent crossings belong to the same mode. For a sharp peak all ${\rm Im}\chi_{\lambda\lambda'}(q,\omega)$ must vanish, too, otherwise that plasmon is Landau-damped. There may also be the case of a weakly Landau-damped, long-lived mode, as we exemplify now.

The qualitative structure of ${\rm Re}\Delta(q,\omega)$ resembles that of all ${\rm Im}\chi_{[aa]}(q,\omega)$ (the middle part of fig. 3 shows $\chi_{[vv]}$). Panel (c), zooming in at very small (q,ω), gives the quantitative information: A sharp mode is close to Δ crossing zero from below, but a peak is lowered significantly compared to this $\Delta = 0$ frequency for low life-times. The damping's magnitude, caused by particle-hole excitations

[6] Reported data differ substantially [38,42], cf. the critical discussion in [43]. We chose refs. [36,44], as they agree nicely.

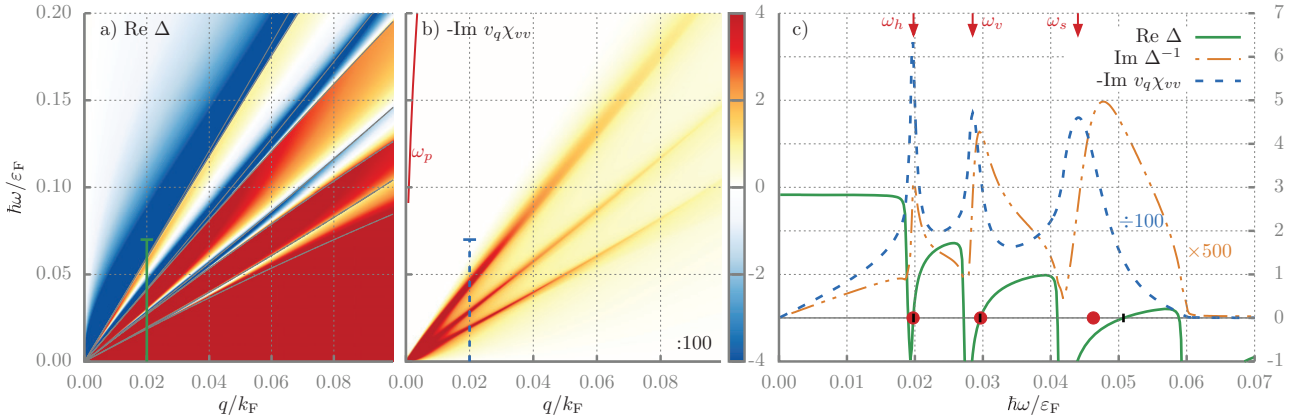

Fig. 3: Partially polarised ($\zeta_\sigma = 0.65, \zeta_\tau = 0.35$) 2DEL. (a) Real part of the denominator $\Delta(q,\omega)$. (b) Imaginary part of the valley-valley response function χ_{vv}, with ω_p labelling the conventional charge plasmon. The vertical axis and the colour bar hold for both (a) and (b); the green and blue vertical lines denote the ($q_0 = 0.02k_F, \omega$)-segment shown in (c): Comparison of $\mathrm{Re}\Delta(q_0,\omega)$ (thick green lines, each "upper" zero is marked by a small black bar) with the scattering contribution from $\mathrm{Im}\chi_{vv}(q_0,\omega)$ (thick dashed blue lines); its peaks ω_h, ω_s, ω_v lie at the red arrows; (ω_p is at higher ω, and the red dots are the corresponding PPA peaks). The loss function, $\mathrm{Im}\Delta^{-1}(q_0,\omega)$ (pale dash–dotted line), shows the "pseudogaps" supporting low decay rates. The the energies of the resulting PPA modes are marked as red dots.

of the 4 components, depends on their respective proportions (dash-dotted, amplified curve): In some ω-regions, termed "pseudogaps", a collective mode is only weakly Landau-damped by a minority component. For 1-valley 2DELs, such a long-lived RPA spin-plasmon was predicted [24], but improving on the RPA shows that it is down-shifted into the high damping regime [25].

Clearly, since ζ_σ and ζ_τ can nowadays be tuned, so can the life-time of collective modes. In fig. 3, ω_h has high strength and weak damping and could thus be of experimental relevance. Precisely predicting (q,ω,ζ_λ) combinations with pronounced peaks requires a better treatment of correlations (see Supplementary Material `Supplementarymaterial.pdf` (SM)), but with the RPA we have narrowed the possibilities.

Another crucial feature of partially polarised 2DELs are lines $\omega(q)$, where the system ignores external stimulation ("anti-resonances") [26,45]. Along $\omega_{\mathrm{mAR}}(q)$ it cannot be excited by a magnetic field; similarly, for $\omega_{\mathrm{vAR}}(q)$ external stress variations cause no response. Formally, this reads

$$\mathrm{Im}\chi_{[ss]}(q,\omega_{\mathrm{mAR}}) = 0 \tag{12a}$$
$$\mathrm{Im}\chi_{[vv]}(q,\omega_{\mathrm{vAR}}) = 0 \tag{12b}$$
$$\mathrm{Im}\chi_{[sv]}(q,\omega_{\mathrm{mAR}}) = 0 = \mathrm{Im}\chi_{[sv]}(q,\omega_{\mathrm{vAR}}). \tag{12c}$$

We show both anti-resonances in fig. 4 for the $(\zeta_\sigma,\zeta_\tau)$ combination of fig. 3 (where they lie at much higher (q,ω)-values than displayed). If $\zeta_\tau > \zeta_\sigma$ the mAR has higher energy than the vAR, merging for $\zeta_\tau = \zeta_\sigma$.

Graphene electrons have a much richer (q,ω)-spectrum than quantum well 2DELs. Increasing ζ_σ at $\zeta_\tau = 0$ drastically broadens the $\sqrt{q}$-plasmon by gapless interband Landau damping; the mAR, where interactions with $n_\downarrow$-spins inhibit an $n_\uparrow$-response, is qualitatively changed from an intraband excitation suppression to one in the interband continuum above the charge plasmon [46]. Certainly,

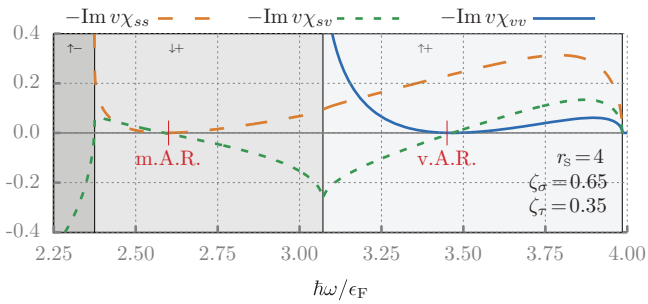

Fig. 4: Magnetic and valley anti-resonance for the system of fig. 3 and $q = 1k_F$: At the zeros of $-\mathrm{Im}\chi_{[ss]}$ and $-\mathrm{Im}\chi_{[vv]}$ (full and long-dashed line, respectively), also the cross-response dissipation, $-\mathrm{Im}\chi_{[sv]}$ (short-dashed line) vanishes.

in partially valley-polarised graphene and TMDs, fascinating dynamic properties await discovery.

Plasmon pole approximation. In order to deepen the understanding of the physics behind these new modes and anti-resonances, the plasmon pole approximation (PPA) (also single-mode or Bijl-Feynman approximation) [1] suits best [26]. We briefly outline it for the spin- and valley-sensitive case. The Lindhard function, eq. (2), involves expectation values of all possible single-particle excitations $\Delta\epsilon^{\lambda\lambda'}_{\mathbf{k},\mathbf{k}+\mathbf{q}}$. The main contribution to this average, its first statistical moment, is equivalent to squeezing all single-particle poles into a single boson-like mode $\omega^0_\lambda(q)$ for each component λ,

$$\chi^0_\lambda(q,\omega) \approx \frac{n_\lambda\, q^2/m^*_\lambda}{\omega^2 - \omega^0_\lambda(q)^2} \tag{13a}$$

(all ω tacitly include a causality ensuring $\mathrm{i}0^+$ and we allow different effective masses for the valleys). The poles $\omega^0_\lambda(q) \equiv \hbar q^2/(S^0_\lambda(q)\,2m^*_\lambda)$ involve the static structure

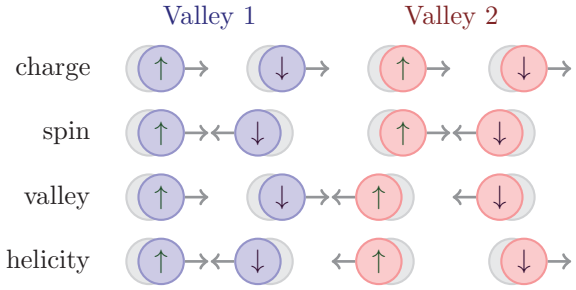

Fig. 5: The four different basic modes of a spin-valley 2DEL.

factors $S^0_\lambda(q)$ of non-interacting fermions. With the diagonal matrices $\underline{\underline{\omega}}$, $\underline{\underline{\omega^0}}$, $\underline{\underline{\mathcal{T}}}$, where $\mathcal{T}_\lambda \equiv n_\lambda q^2/m^*_\lambda$, this reads

$$\underline{\underline{\chi^0}}(q,\omega) \approx \underline{\underline{\mathcal{T}}}(q) \cdot \left(\underline{\underline{\omega}}^2 - \underline{\underline{\omega^0}}(q)^2\right)^{-1}. \tag{13b}$$

Inserting this into the RPA response (4) results in

$$\underline{\underline{\chi}}^{\mathrm{PPA}}(q,\omega) = \underline{\underline{\mathcal{T}}}(q) \cdot \left(\underline{\underline{\omega}}^2 - \underline{\underline{\Omega}}^2(q)\right)^{-1} \tag{14a}$$

$$\underline{\underline{\Omega}}(q)^2 = \underline{\underline{\omega^0}}(q)^2 + \underline{\underline{V}} \cdot \underline{\underline{\mathcal{T}}}. \tag{14b}$$

This is formally identical to the response of 4 harmonic oscillators, with the non-diagonal coupling matrix $\underline{\underline{V}} \cdot \underline{\underline{\mathcal{T}}}$. Calculating the eigenfrequencies $\omega_\lambda(q)$ (the "Bijl-Feynman" modes of a 4-component system), though only numerically possible, is straightforward.

Comparing the weakly coupled, $\zeta_\lambda \gtrsim 0$ case to that of 4 individual oscillators with frequencies $\omega^0_\lambda(q)$, we gain information on the types of modes from the new eigenvectors. The simplest one, an in-phase movement of all oscillators —the sub-species "λ"— is the well-known charge plasmon. It mainly depends on the total electron density[7]. Consequently, it is barely influenced by a spin or valley polarisation. In another mode the oscillators with spin $\uparrow$ move against the $\downarrow$ spins, referred to as "spin plasmon". Analogously, in a "valley plasmon" charge carriers with one valley index oscillate against their antagonists. Since valleys correspond to well-defined momenta in the Brillouin zone, this is not directly interpretable as a real-space oscillation: at any $\mathbf{r}$, both valleys contribute, with an overlaid resonance of their mutual behaviour. Similarly, in the least intuitive mode, oscillators that are distinct in both spin and valley, are in phase[8]. Anticipating its importance in SOC systems, we call this a helicity plasmon. These 4 modes are schematically depicted in fig. 5.

With increased ζ_σ or ζ_τ, depending on the wave vector q, the observed modes get more and more "mixed": their eigenvectors are varied superpositions of the above essential sub-species modes. Consequently, these names should be used *cum grano salis* —*e.g.*, a "spin plasmon" no longer implies that the pseudo-spins are in phase.

[7]Analogously, in-phase movement of mechanical oscillators is dictated by the total mass.

[8]In TMDs this would mean that charges of opposite chirality oscillate against each other.

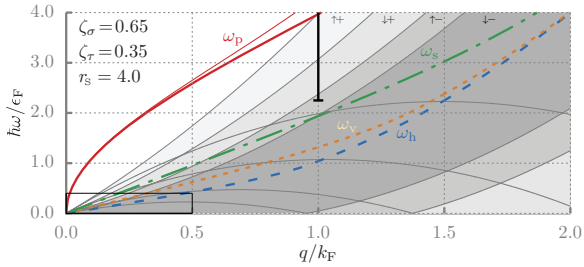

Fig. 6: Charge (ω_p), valley (ω_v), spin (ω_s) and helicity (ω_h) plasmon from PPA (solid red, dash-dotted green, dotted pale, and dashed blue curves, respectively); the thin red line denotes the RPA. The relevant region for the unconventional modes shown in fig. 3 is the rectangle in the left-bottom corner. The black vertical line at $q = 1.0k_\mathrm{F}$ denotes where the RPA spin and valley response functions are shown in fig. 4.

Figure 6 shows a representative PPA result, where we added the single-particle continua. For $\zeta_\tau < \zeta_\sigma$, also $\omega_\mathrm{v} < \omega_\mathrm{s}$ and vice versa, the helicity-plasmon staying at very low energies and deep inside all 4 bands. Thus, at first glance, ω_h appears to be fully damped. However, the RPA result for the same parameters, fig. 3(c)), demonstrates that mainly minority charges are responsible for its life-time: although much larger in number, majority particle-hole excitations only insignificantly effect the helicity-plasmon. Energy transfer within the sub-systems leads to the anti-resonances in fig. 4. Their origin and a PPA↔RPA comparison is discussed in the SM.

Conclusion. – We studied the collective modes of a 2DEL with imbalanced spin as well as valley population in the RPA. For very long wavelengths we confirmed the possible existence of long-lived acoustic modes, as suggested in [24] for the spin plasmon. Depending on the partial polarisations, we find a distinct "valley plasmon", damped only by the component of lowest density (here, $n_{\downarrow-}$). Concerning experimental verification, the dispersion of both, energy as well as life-time, requires a treatment beyond the RPA [25,47,48] before precise predictions can be made. Work in this direction is in progress.

At high energies and intermediate wave vectors two anti-resonances exist: the system cannot follow an external stimulus by magnetic fields or valley manipulation. The related dissipation channels become marginal —an interesting property for applications. Such effects are also expected for electrons in double layers (see, *e.g.*, [49,50]); spin-polarising one layer provides four-components with different inter- and intra-layer coupling. Finding AR-like regions in the excitations of the appealing three-band model of "LAO/STO" interface electrons [51] appears highly interesting, too.

In Dirac 2DELs with partial spin or valley polarisation, the gapless interband Landau damping prevents long-lived modes[9], but the ARs, where a sub-species cannot keep

[9]Thus controlling the partial polarisation of spins or valleys could be exploited to "switch" the plasmon lifetime.

up with stimulation, do not require a gap [46]. Other modern unconventional 2DELs like silicene or TMDs are gapped and thus will share many of the dynamical features presented here. Generalising the study to allow for SOC is expected to yield new insight on the "helicity plasmon" and thus appears most worthwhile.

REFERENCES

[1] Giuliani G. and Vignale G., *Quantum Theory of the Electron Liquid* (Cambridge University Press) 2005.

[2] Nguyen B. H. and Nguyen V. H., *Adv. Nat. Sci.: Nanosci. Nanotechnol.*, **7** (2016) 043001.

[3] Duong D. L., Yun S. J. and Lee Y. H., *ACS Nano*, **11** (2017) 11803.

[4] Choi W., Choudhary N., Han G. H., Park J., Akinwande D. and Lee Y. H., *Mater. Today*, **20** (2017) 116.

[5] Vitale S. A., Nezich D., Varghese J. O., Kim P., Gedik N., Jarillo-Herrero P., Xiao D. and Rothschild M., *Small*, **14** (2018) 1801483.

[6] Sverdlov V. and Selberherr S., *Phys. Rep.*, **585** (2015) 1.

[7] Schaibley J. R., Yu H., Clark G., Rivera P., Ross J. S., Seyler K. L., Yao W. and Xu X., *Nat. Rev. Mater.*, **1** (2016) 16055.

[8] Liu F., Zhou J., Zhu C. and Liu Z., *Adv. Funct. Mater.*, **27** (2017) 1602404.

[9] Bussolotti F., Kawai H., Ooi Z. E., Chellappan V., Thian D., Pang A. L. C. and Goh K. E. J., *Nano Futures*, **2** (2018) 032001.

[10] Dragoman M., Dinescu A. and Dragoman D., *Phys. Status Solidi (a)*, **216** (2019) 1800724.

[11] Lundstrom M., *Fundamentals of Nanotransistors* (World Scientific) 2017.

[12] Sun Y., Thompson S. E. and Nishida T., *J. Appl. Phys.*, **101** (2007) 104503.

[13] Shayegan M., De Poortere E., Gunawan O., Shkolnikov Y., Tutuc E. and Vakili K., *Phys. Status Solidi (b)*, **243** (2006) 3629.

[14] Renard V., Piot B., Waintal X., Fleury G., Cooper D., Niida Y., Tregurtha D., Fujiwara A., Hirayama Y. and Takashina K., *Nat. Commun.*, **6** (2015) 7230.

[15] Gokmen T., Padmanabhan M., Tutuc E., Shayegan M., De Palo S., Moroni S. and Senatore G., *Phys. Rev. B*, **76** (2007) 233301.

[16] Kelly M. J. and Falicov L. M., *Phys. Rev. B*, **15** (1977) 1974.

[17] Bloss W. L., Sham L. J. and Vinter V., *Phys. Rev. Lett.*, **43** (1979) 1529.

[18] Shkolnikov Y. P., Vakili K., De Poortere E. P. and Shayegan M., *Phys. Rev. Lett.*, **92** (2004) 246804.

[19] Das Sarma S., Hwang E. H. and Li Q., *Phys. Rev. B*, **80** (2009) 121303.

[20] Padmanabhan M., Gokmen T. and Shayegan M., *Phys. Rev. B*, **78** (2008) 161301.

[21] Asgari R., Gokmen T., Tanatar B., Padmanabhan M. and Shayegan M., *Phys. Rev. B*, **79** (2009) 235324.

[22] Isihara A. and Ioriatti L., *Int. J. Quantum Chem.*, **22** (1982) 149.

[23] Cole T. and McCombe B. D., *Phys. Rev. B*, **29** (1984) 3180.

[24] Agarwal A., Polini M., Vignale G. and Flatté M. E., *Phys. Rev. B*, **90** (2014) 155409.

[25] Kreil D., Hobbiger R., Drachta J. T. and Böhm H. M., *Phys. Rev. B*, **92** (2015) 205426.

[26] Kreil D., Staudinger C., Astleithner K. and Böhm H. M., *Contrib. Plasma Phys.*, **58** (2018) 179.

[27] Hill A., Mikhailov S. A. and Ziegler K., *EPL*, **87** (2009) 27005.

[28] Yi K. S. and Quinn J. J., *Phys. Rev. B*, **27** (1983) 2396.

[29] Jain J. K. and Das Sarma S., *Phys. Rev. B*, **36** (1987) 5949.

[30] Badalyan S. M., Matos-Abiague A., Vignale G. and Fabian J., *Phys. Rev. B*, **79** (2009) 205305.

[31] Scharf B., Tuan D. V., Žutić I. and Dery H., *J. Phys.: Condens. Matter* , **31** (2019) 203001.

[32] Perez F., *Phys. Rev. B*, **79** (2009) 045306.

[33] Eriksson M., Pinczuk A., Dennis B., Hirjibehedin C., Simon S., Pfeiffer L. and West K., *Physica E*, **6** (2000) 165.

[34] Wang Z., Zhong Z., Hao X., Gerhold S., Stöger B., Schmid M., Sánchez-Barriga J., Varykhalov A., Franchini C., Held K. and Diebold U., *Proc. Natl. Acad. Sci. U.S.A.*, **111** (2014) 3933.

[35] Dharma-wardana M. W. C. and Perrot F. m., *Phys. Rev. B*, **70** (2004) 035308.

[36] Marchi M., De Palo S., Moroni S. and Senatore G., *Phys. Rev. B*, **80** (2009) 035103.

[37] Gokmen T., Padmanabhan M. and Shayegan M., *Phys. Rev. B*, **81** (2010) 235305.

[38] Tanatar B. and Ceperley D. M., *Phys. Rev. B*, **39** (1989) 5005.

[39] Gold A., *Phys. Rev. B*, **50** (1994) 4297.

[40] Takashina K., Niida Y., Renard V. T., Piot B. A., Tregurtha D. S. D., Fujiwara A. and Hirayama Y., *Phys. Rev. B*, **88** (2013) 201301.

[41] Kravchenko S. V., Simonian D., Sarachik M. P., Mason W. and Furneaux J. E., *Phys. Rev. Lett.*, **77** (1996) 4938.

[42] Drummond N. and Needs R., *Phys. Rev. Lett.*, **102** (2009) 126402.

[43] Varsano D., Moroni S. and Senatore G., *Europhys. Lett.*, **53** (2001) 348.

[44] Attaccalite C., Moroni S., Gori-Giorgi P. and Bachelet G. B., *Phys. Rev. Lett.*, **88** (2002) 256601.

[45] Silvestri L., Kalman G. J., Donkó Z., Hartmann P. and Kählert H., *EPL*, **109** (2015) 15003.

[46] Kreil D., Haslhofer M. and Böhm H. M., *Lith. J. Phys.*, **59** (2019) 35.

[47] Moreno J. and Marinescu D. C., *Phys. Rev. B*, **68** (2003) 195210.

[48] Yurtsever A., Moldoveanu V. and Tanatar B., *Phys. Rev. B*, **67** (2003) 115308.

[49] Tanatar B. and Davoudi B., *Phys. Rev. B*, **63** (2001) 165328.

[50] Profumo R. E. V., Asgari R., Polini M. and MacDonald A. H., *Phys. Rev. B*, **85** (2012) 085443.

[51] Faridi A. and Asgari R., *Phys. Rev. B*, **95** (2017) 165419.